Time-Resolved Circular Dichroism Studies of Protein Folding Intermediates of Cytochrome *c*[†]

Eefei Chen, Matthew J. Wood, Anthony L. Fink, and David S. Kliger*

Department of Chemistry and Biochemistry, University of California, Santa Cruz, California 95064

Received September 24, 1997; Revised Manuscript Received January 21, 1998

ABSTRACT: The circular dichroism spectra of cytochrome *c* (cyt*c*) in 4.6 M guanidine hydrochloride (pH 6.5) indicate that the secondary structure in reduced cyt*c* is near-native, whereas in the CO-bound species (COCyt*c*) it is substantially unfolded. Photolysis of COCyt*c* should thus induce large changes in the secondary structure, which can be probed with time-resolved circular dichroism (TRCD) spectroscopy in the far-UV region. Time-resolved absorption (TROA) and TRCD methods were used to study the photolysis reaction of COCyt*c* in efforts to identify structural intermediates in cyt*c* folding on time scales from nanoseconds to seconds. TROA data from the Soret region, similar to previous studies, showed four intermediates with lifetimes of 2, 50, 225, and 880 μs. The 2-μs process is proposed to involve Fe(II)−Met80 coordination. Approximately 7% of the native CD signal was observed in the TRCD signal at 220 nm within 500 ns, with no significant additional secondary structure formation observed. Further folding after 2 μs may be inhibited by ligation of His26/His33 with Fe(II), which is suggested to be associated with the 50-μs phase. The two slowest components, $\tau = 225$ and 880 μs, are attributed to CO rebinding on the basis of mixed-gas experiments. CO rebinding is expected to compete with protein folding and favor the unfolded state. However, when the two CO rebinding lifetimes are extended into milliseconds by reducing the CO concentration, there is still no significant increase in CD signal at 220 nm.

The dynamics of protein folding have been shrouded in controversy that focuses on whether the dominant folding force is hydrogen bonding or hydrophobic interactions. This argument dates back to the 1950s, when Kauzmann (*1*) suggested that protein folding is driven by hydrophobic collapse because hydrogen bond formation with water would strongly favor the unfolded state. This is opposed to the hydrogen bond facilitated folding mechanism that was proposed by Mirsky and Pauling (*2*). To date, this debate remains unsettled, although there have been many efforts toward understanding whether secondary structure formation or hydrophobic collapse comes first in protein folding. One common approach to this question tries to identify and characterize structural intermediates and subdomains of protein folding processes by using a wide variety of techniques, including pulsed H-exchange labeling coupled with proton nuclear magnetic resonance, fluorescence, steady-state circular dichroism (CD), multifrequency calorimetry, and stopped-flow CD methods (*3*−*9*). These studies have focused on folding processes in intact proteins as well as protein fragments and synthesized peptides.

With the above techniques, attempts to capture the different stages of protein folding are limited to the millisecond regime, during which time a large fraction of secondary structure has already formed (*4*, *10*, *11*). By using fast laser spectroscopy coupled with structure-sensitive probes, such as infrared, CD, and fluorescence, it is possible to obtain the time resolution necessary for the study of submillisecond folding events. Studies using laser temperature jump (T-jump), electric field jump, and resonant ultrasound techniques, all of which have a time resolution of several nanoseconds, have already observed helix to coil relaxation lifetimes in the range of 20 ns to 15 μs for homopolymers (*12*−*19*). Recently, nanosecond folding transients were observed in temperature-induced perturbations of a 21-residue alanine-based peptide (*20*, *21*), apomyoglobin (apoMb) (*22*−*24*), barstar (*25*), and ribonuclease A (*26*).

Unlike laser T-jump experiments, time-resolved ligand photolysis studies of protein folding have been limited by the availability of biomolecules with chromophores where unfolding or refolding can be triggered by a photoevent. A biochemical system based on cytochrome *c* (cyt*c*) has been developed where folding can be optically triggered through a heme ligand photodissociation reaction (*27*). As an electron shuttle of the mitochondrial electron transport chain, cyt*c* undergoes changes in the oxidation state of the heme iron under physiological conditions. Unlike heme proteins such as myoglobin (Mb), which can undergo ligand dissociation, both the reduced (redCyt*c*) and oxidized (oxCyt*c*) forms of cyt*c* are 6-coordinate with His18 and Met80 in the axial positions. In the presence of the denaturant guanidine

[†] This work was supported by NIH Grant GM-35158 (D.S.K.), NSF Grant MCB-9507280 (A.L.F.), and in part by a University of California President's Postdoctoral Fellowship (E.C.).

* To whom correspondence should be addressed.

[1] Abbreviations: CD, circular dichroism; ApoMb, apomyoglobin; cyt*c*, cytochrome *c*; GdnHCl, guanidine hydrochloride; CO, carbon monoxide; redCyt*c*, reduced form of cyt*c*; COCyt*c*, CO-bound cyt*c*; TROA, time-resolved absorption; TRCD, time-resolved circular dichroism; NaP, sodium phosphate; oxCyt*c*, oxidized form of cyt*c*; TRFL, time-resolved fluorescence.

S0006-2960(97)02369-6 CCC: $15.00
Published on Web 03/28/1998

hydrochloride (GdnHCl), carbon monoxide (CO) can bind to redCyt*c* at the native Met80 position to form a photolabile iron−CO [Fe(II)−CO] bond. As demonstrated by steady-state fluorescence and CD studies (*27*), the presence of CO favors a relatively unfolded protein conformation of cyt*c*. Thus, at appropriate denaturant concentrations, the redCyt*c* species has near-native protein secondary structure and the CO-bound cyt*c* (COCyt*c*) has a denatured conformation.

The COCyt*c* refolding reaction can be initiated by photolysis of the CO ligand, which preferentially binds to the heme iron at the sixth axial coordination position that is occupied by Met80 in the native protein. Photolysis of the CO bond leads to an equilibrium between refolding, when CO is deligated, and unfolding, as the ligand rebinds. Time-resolved optical absorption (TROA) methods have been used by Jones et al. (*27*) to study ligand rebinding and protein folding in the COCyt*c* system. Kinetic modeling of their data suggests that transient binding of non-native ligands (His26, His33, and Met65) and the native Met80 ligand to the heme occurs on a microsecond time scale prior to protein folding. With further investigations of this system, Hagen et al. (*28*, *29*) suggested that interactions of the heme with Met80 or Met65 and His26 and/or His33 are formed with time constants of 3−4 and 120 μs, respectively. Similar experimental conditions were reported under which folding can be initiated in unfolded ferricytochrome *c* by electron transfer (*30*, *31*). In these electron injection studies, a 40-μs process was reported and associated with the formation of a molten globule intermediate. Since the molten globule species has been described as having near-native secondary structure content, a significant increase in the CD signal at 220 nm should be observed if there is such a refolding intermediate. Using sample conditions similar to those reported by Jones et al. (*27*), we present here the results of near- and far-UV time-resolved circular dichroism (TRCD) investigations. This structurally sensitive technique was used to probe the global protein secondary structural changes that occur upon photolysis of COCyt*c* to test hypotheses which have been proposed for folding intermediates of cyt*c* that are based on less structurally sensitive measurements.

MATERIALS AND METHODS

Sample Preparation. Horse heart and tuna cyt*c* of >99% purity, purchased from Sigma Chemical Co., and sodium hydrosulfite (dithionite), from both Sigma Chemical Co. and Fluka, were used without further purification. Ultrapure GdnHCl was obtained from ICN Biomedicals Inc.; sodium chloride (NaCl) and monobasic (Na_2HPO_4) and dibasic (NaH_2PO_4) sodium phosphates were purchased from Fisher Scientific.

Samples were prepared with final concentrations of 40−106 μM cyt*c*; 4.6, 5.5, or 6 M GdnHCl; and 0.1 M sodium phosphate (NaP) and a final pH of either 6.5, 4.1, or 1.7. At pH 1.7 the cyt*c* samples were prepared in the presence of 1 M NaCl. The final concentration of sodium dithionite was never more than 5 times the concentration of cyt*c*, because sodium dithionite has an absorption band at ca. 314 nm that can interfere with studies in the far- and near-UV regions. These solutions were deoxygenated with either Ar (for the CO-unbound reduced form, redCyt*c*) or CO (for COCyt*c*) gas for several hours before the experiment. Solid oxCyt*c* and sodium dithionite were separately deoxygenated in dry sealed flasks for approximately 30 and 15 min, respectively, before addition of oxygen-free buffer. The COCyt*c* solution was then transferred to a deoxygenated flow apparatus that was maintained under CO gas pressure throughout the experiment.

The flow apparatus was connected to either 0.3, 0.5, or 2 mm path length cells for experiments in the Soret and far- and near-UV regions. These path lengths gave absorbances of approximately 1 at 412, 222, and 272 nm, respectively, for the sample concentration used. The cells employed fused silica windows and a heating/cooling jacket for temperature control. All experiments were performed with the sample stabilized at 40 °C. Since fluctuations in the temperature of the cell windows result in birefringence artifacts that mask the CD signal, it was necessary to equilibrate the temperature of the cell at 40 °C for at least 1 h before collecting TRCD data. The COCyt*c* sample was flowed through the cell for approximately 30−45 min to allow the sample temperature to reach equilibrium. The results of experiments performed with and without flowing the sample showed no differences. For most TROA experiments the sample was flowed to avoid the buildup of photodegradative products. To be certain that the laser photolyzed undegraded COCyt*c* each time, the earliest delay time (140 ns) was measured after every 5−10 time points and compared to the 140-ns difference TROA spectrum obtained at the beginning of the experiment. Because continuous flow during TRCD experiments can introduce artifacts to the spectrum, new sample was flowed into the cell only after each scan. Data collection alternated between a time-resolved measurement and an initial-state CD measurement of COCyt*c* to verify that the sample had not degraded. In addition, a steady-state absorption spectrum of COCyt*c* was measured periodically on a Shimadzu UV-2101PC spectrophotometer (Columbia, MD) during each experiment to ensure sample integrity.

Steady-State Circular Dichroism Experiments. Steady-state CD measurements were performed on an AVIV 62 DS circular dichroism spectrometer (AVIV Associates, Lakewood, NJ). The cyt*c* samples were allowed to temperature equilibrate for ∼15 min at 40 °C before data were collected. The CD data were accumulated for 5 s every 1 nm, with a 1.5-nm bandwidth.

Photolysis Experiments. Photolysis of the sample was initiated by a Q-switched DCR-1 Nd:YAG laser that generates ∼7-ns (full width at half-maximum), 26−27-mJ, 532-nm pulses with a repetition rate of 1 or 2 Hz. The unfocused laser beam was approximately 8 mm in diameter and entered the cell at a 30° angle relative to the probe beam propagation axis, which is normal to the face of the sample cell. Changes in the sample that are induced by photoexcitation were probed with a xenon flash lamp.

For TRCD experiments the initially unpolarized probe beam is collimated before it is linearly polarized by a MgF_2 Rochon polarizer, P1. The linearly polarized light is converted to highly eccentric elliptical light by passing the probe beam through a birefringent, fused silica strain plate (SP). The SP introduces a retardation, δ, of approximately 1−2° along an axis oriented ±45° relative to the linear polarization axis, and rotation of SP by 180° produces left (−45°) and right (+45°) elliptically polarized (LEP and REP, respectively) light. Changes in the ellipticity of LEP and

Table 1: Kinetics of Horse Heart COCyt*c* Photolysis[a]

method	time constants (μs)/amplitudes			
	$\tau(1)$	$\tau(2)$	$\tau(3)$	$\tau(4)$
time-resolved absorption spectroscopy				
Soret	2/0.08	50/0.30	225/0.25	880/0.35
3:1, Ar:CO	2/0.09	70/0.30	640/0.26	2200/0.34
tuna heart	2/0.09	40/0.11	250/0.56	710/0.24
near UV	2.5/0.17	75/0.18		745/0.54
time-resolved circular dichroism spectroscopy				
near UV	2.5/0.14	65/0.15		745/0.63

[a] Experimental conditions: 4.6 M GdnHCl, pH 6.5, and 40 °C (1 atm CO) for horse cyt*c* unless otherwise noted.

REP that are induced by a circularly dichroic sample are measured by passing the probe beam through an analyzing linear polarizer (P2) that is oriented 90° to P1. The transmitted signal is focused onto the slit of a spectrograph that is coupled to an optical multichannel analyzer.

The TROA apparatus is a modification of the TRCD configuration, where P1, P2 and SP are removed. Further details of the TROA and TRCD apparatus can be found in previous publications (*32*−*35*).

Time-Resolved Measurements. TROA data were collected at approximately 5 logarithmic delay times per decade between 140 ns and 1 μs, at 10 logarithmic delay times per decade between 1 μs and 10 ms, and then at 20, 50, 80, 100, 200, 500, 800, and 1000 ms. The time resolution of the TROA system was 140 ns. Approximately 46 time points were measured for each TROA experiment. Spectra were measured at a repetition rate of 2 Hz for time delays between 140 ns and 200 ms after photolysis, and at 1 Hz for time delays longer than 200 ms. Using these repetition rates and flowing the sample during the experiment helped ensure that each laser shot photolyzed only COCyt*c*. TROA data were analyzed in the form of difference spectra, $A(t) - A(t_o)$, where t represents the time delay after photolysis, and $A(t_o)$ is the spectrum of the unphotolyzed sample.

Near-UV TRCD data were collected at 420 and 630 ns; 1, 2, 5, 10, 20, 32, 40, 50, 63, 100, 200, 320, 400, 500, 630, and 800 μs; and 1, 2, 5, 10, and 20 ms after photoinitiation of the reaction. Approximately 2000 scans were averaged at each time delay. Data were analyzed in the form of difference spectra of $S(t) - S(t_o)$, where $S(t)$ is the CD signal at various time delays after photolysis, and $S(t_o)$ is the initial-state CD signal. Far-UV TRCD data were collected at 500 ns; 2, 10, 100, and 500 μs; and 1, 5, and 10 ms after initiation of folding, with approximately 10 000 averages accumulated at each time delay. Data in both regions were collected with a 2-Hz repetition rate because the TRCD signal returns to the initial-state CD signal in less than 500 ms.

Data Analysis. The TROA and TRCD data were analyzed by using singular value decomposition (SVD) and global analysis methods. Because details of SVD and global analysis applied to heme proteins have been published elsewhere (*36*, *37*), they will only be described briefly here. Given a set of unimolecular photolysis reactions with spectrally distinguishable intermediates, the time evolution of these species can be probed with the spectral changes that occur after photolysis. SVD is a matrix approach that distinguishes the experimental noise from the spectral information and identifies the minimum number of independent species required to describe spectral variations in the TROA or TRCD difference data. The data matrix (**A**) is decomposed into mathematically independent spectral (**U**) and temporal (**V**) components, each of which is weighted with a singular value (**S**) that defines its importance to the data, $\mathbf{A} = \mathbf{USV}^T$.

The time course of N spectral intermediates is followed with global kinetic analysis. Using this method, the data can be expressed as a function of the difference extinction coefficients of the intermediates and final product relative to the unphotolyzed species and the concentration of the intermediates and final product, $\mathbf{A}(\lambda,t) = \epsilon(\lambda)\mathbf{C}(t)$. The time-dependent intermediate concentrations can be written as $\mathbf{C} = C_0\mathbf{KT}$, where C_0 is the concentration of the unphotolyzed species; $\mathbf{C} = \{C_1(t), C_2(t), ..., C_N(t), C_{N+1}(t)\}^T$; and **K** is an $(N + 1) \times (N + 1)$ matrix that is determined by the reaction mechanism and the apparent rate constants k_1, k_2, ..., k_N. As a result, the data can be expressed as $\mathbf{A} = C_0\epsilon(\lambda)\mathbf{KT}(t)$. Using global kinetic methods, the intermediate spectra (ϵ), the corresponding decay rate constants (**T**), and the reaction mechanism (**K**) can be identified. When **B**, the spectral components or "*b*-spectra", is defined as $C_0\epsilon(\lambda)\mathbf{K}$, the raw data can be fit to a product of time (**T**) and spectral (**B**) components, $\mathbf{A} = \mathbf{BT}$, that are identified with each intermediate.

SVD and global analysis were performed with the mathematical software package Matlab (Pro-Matlab, The Math Works, Inc., South Natick, MA).

RESULTS

Because the partially unfolded cyt*c* system is sensitive to pH, temperature, and GdnHCl concentration, the Soret TROA experiments reported by Jones et al. (*27*) were repeated to provide a point of reference for the TROA experiments in the near-UV and visible regions and the TRCD studies in the near- and far-UV regions. The results of these studies are summarized in Table 1. The data in the figures presented below were obtained from experiments on horse heart cyt*c* unless otherwise noted.

Figure 1A shows a typical set of TROA data measured at 40 °C in the Soret region, which consists of 32 averages at each time delay after photolysis. The difference TROA spectra show a negative feature that follows the disappearance of the partially unfolded state and a positive feature that represents the corresponding appearance of the photoproduct. The spectra show a distinct blue shift of the absorbance maximum from ca. 430 to 425 nm as a function of time. Using SVD and global analysis methods, the data were fit reliably to four exponential processes with lifetimes of 2, 50, 225, and 880 μs, and corresponding relative amplitudes of 0.08, 0.30, 0.25, and 0.35 (Table 1). The time-

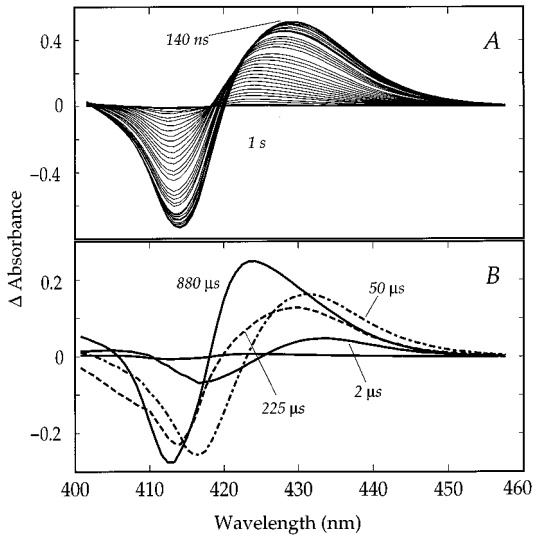

FIGURE 1: (A) Soret TROA difference spectra, $A(t_i) - A(t_o)$, were measured at 46 time delays after initiation of refolding, with each spectrum representing 32 averages per time point. Data sets of TROA spectra collected with 32 averages were analyzed separately and used to calculate the average value for each exponential lifetime and its corresponding standard deviation. A 5-nm blue shift is observed in the wavelength maximum of the positive absorption from 430 to 425 nm. These data were collected using 106 μM COCyt*c* with either a 0.5 or a 0.3 mm path length cell, and the temperature was stabilized at 40 °C. (B) *b*-Spectra corresponding to the four exponential components (2, 50, 225, and 880 μs) detected by SVD and global analysis methods.

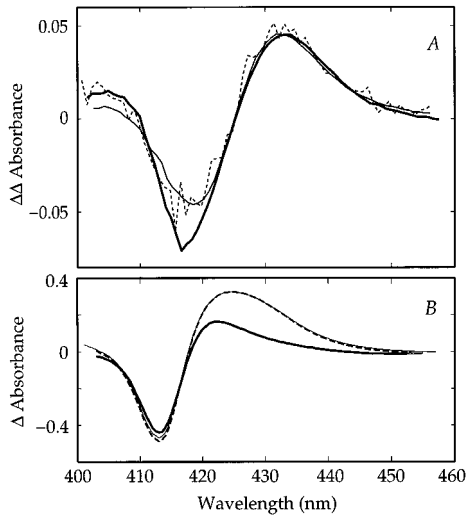

FIGURE 2: (A) *b*-Spectrum associated with the 2-μs process (thick line) compared to *b*-spectra calculated from Soret TROA data measured for photolysis of COCyt*c* in 6 M GdnHCl (pH 4.1, 40 °C, $\tau = 2$ μs, - - -) and redCyt*c* in 4.6 M GdnHCl (pH 6.5, 40 °C, $\tau = 2.4$ μs, thin line). The spectra were obtained using 106 μM cyt*c* in a 0.5-mm flow cell. (B) Equilibrium difference absorption spectrum of redCyt*c* and COCyt*c* (4.6 M GdnHCl, thick line) compared to the difference spectrum of photolyzed COCyt*c* measured at 140 ns and unphotolyzed COCyt*c* (- - -). The difference TROA spectrum measured 140 ns after COCyt*c* photolysis can be overlaid with the equilibrium difference spectrum of redCyt*c* and COCyt*c* obtained in 5.5 M GdnHCl (thin line). Spectral differences reveal the presence of red-shifted photoproduct(s), as well as redCyt*c*, 140 ns after photolysis.

dependent spectral changes that accompany the intermediate processes (*b*-spectra) are shown in Figure 1B. Analysis of Soret TROA data measured for tuna COCyt*c* also gives four intermediate species with similar lifetimes, 2, 40, 250, and 710 μs. In tuna cyt*c* the His33 found in horse cyt*c* is replaced by a Trp residue. Only the Soret TROA results from tuna COCyt*c* measurements will be discussed in this article.

Under mixed-gas conditions of 3:1 argon to CO, the TROA data are fit to four exponential processes (Table 1), but with time constants of 2, 70, and 640 μs and 2.2 ms. The first two exponentials do not appear to be significantly affected by the decrease in CO concentration. However, because the last two processes are extended by a factor of 2.5−3-fold compared to the lifetimes measured under experimental conditions of 1 atm CO, they are assigned to bimolecular CO rebinding processes.

The *b*-spectra shown in Figure 1B suggest that the appearance of the earliest COCyt*c* photoproduct is rapidly followed by religation within 2 μs of a small percentage of Fe(II). As suggested by Jones et al. (*27*), there are several possible candidates for this religation process, including native Met80 and non-native His26, His33, and Met65. Although it can be concluded through mixed-gas studies that this bond is not formed with CO, the identity of the ligand involved in the 2-μs process is still under investigation. However, the results of various TROA studies, designed to eliminate specific ligands as possible candidates for the 2-μs process, provide some idea of which ligand is involved. In the absence of GdnHCl, redCyt*c* shows no product of photolysis. However, when redCyt*c* is prepared in the presence of 4.6 M GdnHCl (pH 6.5, 40 °C), a photoproduct is observed. The resulting Soret TROA data on redCyt*c* can be fit to a single-exponential process with a lifetime of approximately 2.4 μs. As shown in Figure 2a, the *b*-spectrum associated with this 2.4-μs component can be overlaid with the *b*-spectrum of the 2-μs process obtained from photolysis of COCyt*c* in 4.6 M GdnHCl (pH 6.5, 40 °C), suggesting that the latter process involves the formation of an Fe(II)−Met80 ligation. In Figure 2A the 2-μs *b*-spectrum from photolysis of COCyt*c* in 4.6 M GdnHCl (pH 6.5, 40 °C) is also compared to the *b*-spectrum associated with a 2-μs component detected in Soret TROA experiments on COCyt*c* in 6 M GdnHCl (pH 4.1, 40 °C), under which conditions His33 and His26 should be protonated (*38*−*40*). The results from the above experiments help to eliminate His as the ligand involved in the 2-μs process. Also comparable, but not shown, are the *b*-spectra for similar processes obtained from photolysis data on COCyt*c* in 4.6 M GdnHCl at pH 1.7 (1 M NaCl, 40 °C, $\tau = 3.5$ μs), where all three His residues should be protonated, and tuna COCyt*c* in 4.6 M GdnHCl at pH 6.5 (40 °C, $\tau = 2$ μs), where His33 is replaced by tryptophan.

Figure 2B compares the Soret equilibrium difference absorption spectra of redCyt*c* and COCyt*c* measured in the presence of 4.6 and 5.5 M GdnHCl at 40 °C (pH 6.5) with the difference TROA spectrum measured 140 ns after photolysis. In contrast to the equilibrium spectrum measured in 4.6 M GdnHCl, the 140-ns TROA spectrum can be overlaid with the equilibrium difference spectrum measured in 5.5 M GdnHCl. These results suggest that the environment of the heme group in the photoproduct 140 ns after photolysis is unlike that in redCyt*c* but is similar to the unfolded conditions that are induced in the protein by the presence of 5.5 M GdnHCl. The spectral differences in

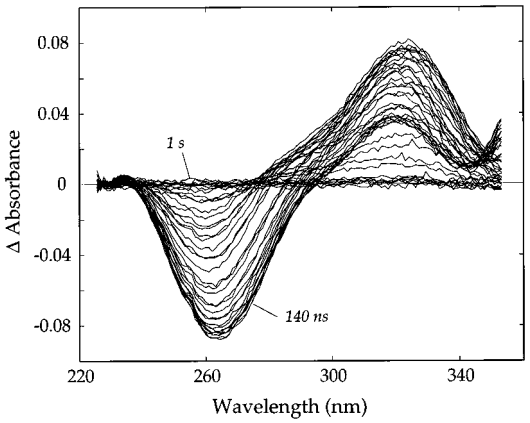

FIGURE 3: TROA difference absorption spectra, $A(t_i) - A(t_o)$, in the near-UV region. Near-UV spectra, each comprising 32 averages, were collected at 40 °C using a 2 mm path length flow cell and 106 μM COCyt*c*. All data sets include measurements at 46 time delays after photolysis of COCyt*c*. The TROA data were analyzed by focusing on each band alone in the wavelength regions of 220−290 and 290−350 nm, as well as including both bands. Only three exponential processes (2.5, 75, and 745 μs) were detectable.

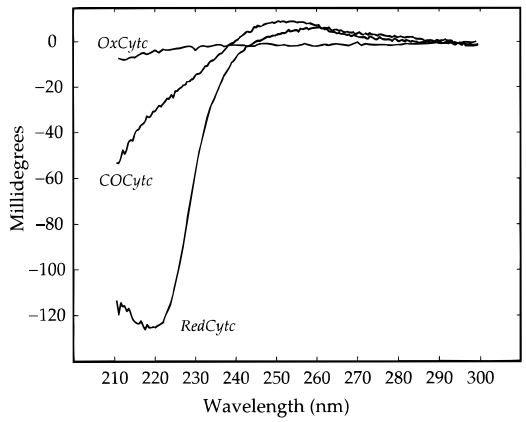

FIGURE 4: Steady-state circular dichroism spectra of cyt*c* in 4.6 M GdnHCl. CD spectra were measured for oxCyt*c*, COCyt*c*, and redCyt*c* in 4.6 M GdnHCl at 40 °C. These spectra emphasize the potential that COCyt*c* has for studying protein folding, initiated by photolysis of the Fe(II)−CO bond, using time-resolved methods. Each spectrum was collected with 5 s integration time every 1 nm using a bandwidth of 1.50 nm. The samples were allowed to temperature equilibrate for approximately 15 min before data collection. These CD spectra were measured using a 1 mm path length cell and a sample concentration of 106 μM.

Figure 2B are expected because the interactions between the heme group and an unfolded versus a folded protein structure are likely to be different, and they can be reflected in the absorption spectra.

Figure 3 shows difference TROA data collected in the near-UV region. Each spectrum represents an average of 32 scans at each time delay after photolysis. The absorbance minimum shows a similar time-dependent 5-nm blue shift that is observed in the Soret region, while the positive feature is unusual in that the absorbance first increases and then decreases as the time delay progresses from 140 ns to 1 s. The time dependence of the spectral changes was determined by analyzing the entire wavelength range measured (220−360 nm) as well as the 260-nm (220−290 nm) and 320-nm (290−360 nm) bands separately. SVD and global analysis generate similar three exponential fits for all three wavelength ranges (Table 1). The lifetimes associated with each of the three exponential processes, 2.5, 75, and 745 μs, were obtained by averaging the results from 7 experiments. Attempts to fit an additional exponential generate either irreproducible lifetimes or two lifetimes with the same value.

In 4.6 M GdnHCl the fraction of unfolded protein in COCyt*c* is approximately 0.95, whereas for redCyt*c* only about 10% of the protein is unfolded. These differences are reflected clearly in the equilibrium CD spectra of COCyt*c* and redCyt*c*. As demonstrated in Figure 4, there is an approximately 4-fold larger CD signal at 220 nm for the CO-unbound redCyt*c* species. This result is the basis for the TRCD studies in the near- and far-UV regions. The CD spectra are cut off at 210 nm because the 4.6 M GdnHCl present in the cyt*c* sample absorbs too much of the light below 210 nm for accurate measurements. This is also the case for the TRCD data.

Figure 5A shows TRCD data measured for COCyt*c* in the near-UV region at 23 time delays after photolysis. Each spectrum represents an average of approximately 2000 scans. The TRCD data were analyzed as difference spectra (Figure 5B) between the photoproduct spectra and the initial-state spectrum. The time-dependent spectral changes can be described by three exponential components with lifetimes

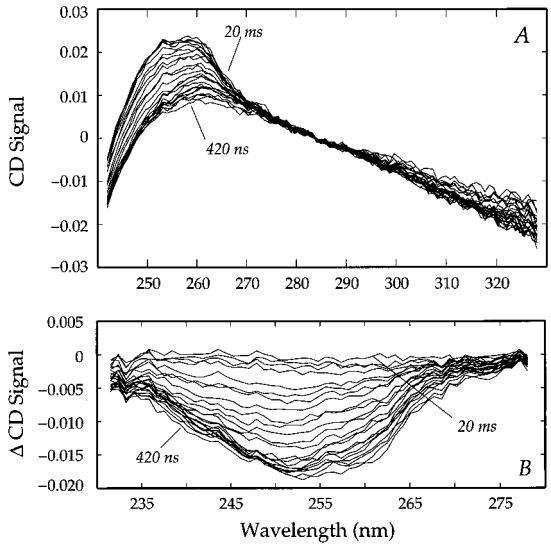

FIGURE 5: TRCD spectra of COCyt*c* [$S(t_o)$] and COCyt*c* photoproducts [$S(t_i)$] measured in the near-UV region. Near-UV TRCD spectra are shown as absolute CD signals (A) and as difference spectra, [$S(t_i) - S(t_o)$]. (B) The data in part A show spectra averaged over ca. 2000 scans at each of the 23 time delays after photolysis. Since the experiments were performed using an absorbance value of ∼1 at 260 nm, there is large sample absorption at wavelengths shorter than 250 nm that lead to slight distortions of the CD signals near 250 nm. Consequently, only data in the 255−300-nm wavelength range were used in the analysis. Similar to the near-UV TROA results, the analysis revealed three exponential components with time constants of 2.5, 65, and 745 μs. These spectra were measured using a 2 mm path length flow cell and 106 μM sample.

of 2.5, 65, and 745 μs (Table 1). The time resolution of these experiments was 420 ns, which allows detection of CD changes associated with the 2-μs process observed in the Soret TROA data.

Whereas the steady-state CD spectra shown in Figure 4 suggest that significant changes in the far-UV CD signal should be observed upon cleavage of the Fe(II)−CO bond, only small changes were detected in the far-UV TRCD experiments. Figure 6 shows the ground-state CD spectra

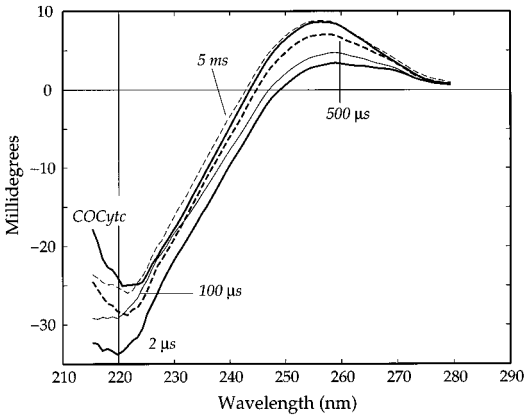

FIGURE 6: Far-UV TRCD spectra of COCyt*c* and its photoproducts. Approximately 10 000 scans were averaged for the far-UV TRCD spectra, which were measured at 500 ns; 2, 10, 100, and 500 μs; and 1, 5, and 10 ms after initiation of refolding. Since there are only small changes in the magnitude of the TRCD signal, only a few spectra are shown (2, 100, and 500 μs and 5 ms). The spectrum measured at 500 ns is not significantly different from that obtained at 2 μs. By 1 and 5 ms the TRCD spectra overlay the ground-state CD spectrum of COCyt*c*. These spectra were obtained with 106 μM COCyt*c* samples and a 0.5 mm path length flow cell.

for COCyt*c* and TRCD spectra measured at 2, 100, and 500 μs and 5 ms after ligand photolysis. The magnitude of the 220-nm TRCD signal 500 ns after photolysis (7% of the native CD signal, not shown) is approximately 85% of the magnitude of the CD signal at 2 μs, which corresponds to 8% of the native CD signal. At 5 ms after photolysis the TRCD spectrum overlays the initial-state COCyt*c* spectrum. As with the steady-state CD spectra, the light is limited at wavelengths below 210 nm because of GdnHCl absorption. Thus, we focus on the results measured at wavelengths longer than 215 nm.

DISCUSSION

The presence of GdnHCl in an oxCyt*c* solution denatures the native protein while the heme Fe(III) maintains a low-spin state with both axial sites occupied by strong field ligands (*38*). Under these denaturing conditions the native Fe(III)−Met80 bond can be displaced by CO with the introduction of sodium dithionite, which reduces Fe(III) to Fe(II). The concentration midpoints for COCyt*c* and redCyt*c* folding in GdnHCl are considerably different. Therefore, it is possible to find a concentration of GdnHCl where in the presence of CO the fraction of unfolded protein is greater than 0.9 and in the absence of CO the fraction of unfolded protein is less than 0.1. In 4.6 M GdnHCl (pH 6.5, 40 °C) it has been shown that there is an approximately 4-fold larger CD signal at 220 nm for redCyt*c* than for COCyt*c*. This corresponds to near-native secondary structure in the redCyt*c* species and significantly unfolded structure in COCyt*c*. From this result it follows that photolysis of Fe(II)−CO should initiate folding of the partially unfolded protein structure found in COCyt*c* until a CO ligand rebinds to Fe(II), reforming COCyt*c* and favoring the unfolded protein structure. Therefore, TROA and TRCD methods were used to examine the photolysis reaction of COCyt*c* in an effort to identify structural intermediates that are involved in the cyt*c* folding process between 140 ns and 1 s. In these studies two bimolecular rebinding processes, along with a possible misligation step, appear to compete with protein folding during the early stages of secondary structure formation in cyt*c*.

We examined the effect of CO deligation on the heme−protein interaction with TROA studies of COCyt*c* (4.6 M GdnHCl, pH 6.5, 40 °C) in the Soret and near-UV regions. An immediate observation is that the difference absorption spectra of redCyt*c* and COCyt*c* measured at equilibrium and 140 ns after photolysis do not overlay. However, the TRCD spectrum obtained 140 ns after photolysis can be overlaid with the equilibrium redCyt*c* and COCyt*c* difference spectrum measured in the presence of 5.5 M GdnHCl (pH 6.5, 40 °C). According to the folding curve for redCyt*c*, the protein in 5.5 M GdnHCl is almost completely unfolded, whereas it is approximately 10% unfolded in 4.6 M GdnHCl (our data, not shown; Jones et al., ref *27*, Figure 1, inset). Thus, the TROA difference spectrum measured at 140 ns probably reflects a heme surrounded by a denatured protein structure. This is supported by far-UV TRCD data which indicate that the protein has not folded to any significant extent at 140 ns.

CO Rebinding Processes. Using SVD and global analysis methods, the spectral changes observed in the Soret TROA data were fit to four exponential components with lifetimes of 2, 50, 225, and 880 μs. Through mixed-gas experiments the 225- and 880-μs processes have been assigned to bimolecular CO rebinding (Table 1). Analysis of near-UV TROA data generated only three of the four exponential time constants (2.5, 75, and 745 μs) observed in the Soret region. The absence of a 225-μs component may be explained in at least two ways. First, if the 225-μs transient is spectrally similar to either the photoproduct or the CO-bound species in the near-UV, it may not be detectable. Alternatively, the lack of a 225-μs transient could reflect the sensitivities of the Soret and near-UV absorptions to different types of molecular interactions, which would suggest that the CO rebinding associated with the 225-μs intermediate involves different structural interactions than in the slower process of CO rebinding. In near-UV TRCD studies we find that the data are also fit to only three processes (2.5, 65, and 745 μs). The apparent silence of the 225-μs process in this region supports the idea that CO rebinds to structurally different species in the two processes of rebinding. The 225-μs transient reflects CO rebinding to a species that has weak interactions between the heme group and nearby aromatic residues since it is not detectable in the near-UV data. In contrast, the 745-μs process involves CO rebinding to a species that has detectable heme−aromatic group interactions. The origin of two different conformational populations is discussed further below.

The 2- and 50-μs Processes. In the kinetic model described by Jones et al. (*27*) several non-native ligands (such as His26, His33, and Met65) were suggested to compete for transient binding to the heme before displacement by CO. The idea of a transient non-native, six-coordinate heme species is consistent with the results of TROA studies on redCyt*c* and COCyt*c* performed under varying conditions of GdnHCl concentration and pH. Because we can detect only a single-exponential process (τ = 2.4 μs) from the redCyt*c* (4.6 M GdnHCl, pH 6.5, 40 °C) photolysis data, it can be assigned to the recombination of the photolyzed ligand. In redCyt*c* we expect the photosensitive ligand to

be Met80, although it is possible that in the presence of 4.6 M GdnHCl Met65 occupies this site.

The results of several studies, including photolysis of redCyt*c*, support the suggestion that the 2-μs process identified in COCyt*c* photolysis studies is due to ligation of Fe(II) with either Met80 or water, rather than to coordination with the non-native His26 and/or His33 residues, or the recombination of a photolyzed Fe(II)−His18 bond. First, in TROA studies of COCyt*c* in 6 M GdnHCl (pH 4.1, 40 °C), a 2-μs component is observed. As shown in Figure 2A, the *b*-spectrum for the 2-μs process measured from COCyt*c* (6M GdnHCl, pH 4.1, 40 °C) photolysis can be overlaid with the 2.4-μs *b*-spectrum detected in the redCyt*c* (4.6 M GdnHCl, pH 6.5, 40 °C) photolysis and the 2-μs *b*-spectrum observed in COCyt*c* (4.6 M GdnHCl, pH 6.5, 40 °C) photolysis. In 6 M GdnHCl (pH 4.1) His26 and His33 are expected to be protonated (*8*, *38*−*42*) and unable to form His18−Fe(II)−His26/33 (bis-His) complexes. Therefore, detection of a 2-μs component in COCyt*c* (6 M GdnHCl, pH 4.1, 40 °C) suggests that His26/33 can be eliminated as candidates for the 2-μs process observed from photolysis of COCyt*c* in 4.6 M GdnHCl. Second, when the pH is dropped from 6.5 to 1.7, the data obtained from photolysis of COCyt*c* in 4.6 M GdnHCl exhibit a 3.5-μs process, with a *b*-spectrum that can be overlaid with the spectra in Figure 2A. Because all His residues, including the proximal His18, should be protonated at pH 1.7 (*38*), the recombination of a photolyzed Fe(II)−His18 bond can also be eliminated. Finally, the possibility of a water ligand in the 2-μs process is addressed by considering the cyt*c* acidification studies of Babul and Stellwagen (*43*). In these studies it was shown that the strong field ligands (Met80 and His18), even when oxCyt*c* is in 6 M GdnHCl or 9 M urea, can only be replaced by weak field ligands of the solvent when the protein solution is acidified. The observation of a 2-μs component (with corresponding *b*-spectra that can be overlaid) at pH 1.7 and 4.1, as well as pH 6.5, suggests that water cannot yet be completely excluded as a possible transient ligand.

The 50-μs process has a lifetime that is similar in value to the 40-μs component that was observed upon reduction of oxCyt*c* (*30*). In those electron-transfer experiments the 40-μs process was interpreted as a molten globule intermediate. Different identities for the processes in these two experimental systems are possible because of the different forms of cyt*c* studied (oxCyt*c* versus redCyt*c*), the different methods used to initiate folding (ligand photolysis versus electron transfer), and the sensitivity of cyt*c* to experimental conditions such as pH, temperature, and the concentration of GdnHCl. However, the results of our experiments do not support the formation of a molten globule intermediate on that time scale, but suggest that the 50-μs component is associated with coordination of His26/33 with Fe(II).

Evidence for a transient (50 μs) Fe(II)−His26/33 ligation comes from the results of Soret TROA studies on COCyt*c* from tuna, which differs from horse COCyt*c* by substitution of His33 with tryptophan. These data could be fit with four exponential decays having lifetimes of 2, 40, 250, and 710 μs. The amplitude of the 40-μs process is approximately 33−43% of the magnitude of the 50-μs process observed in photolysis studies of horse COCyt*c*, while that for the 2-μs species is unaffected. The decrease in intensity of the 40-μs component is consistent with the absence of His33 and suggests that His33 is more accessible than His26 to Fe(II). His26 is only 8 residues from the proximal His18 at the fifth axial site, and it is likely to be more sterically hindered from binding at the sixth axial position than is His33. This is consistent with recent studies of denatured cyt*c* variants which implicate His33 as the dominant sixth axial ligand (*44*). The 50-μs component may be comparable to the bis-His intermediate that was recently reported in folding studies of oxCyt*c* in 4.4 M GdnHCl (*45*). That study monitored the folding intermediates with resonance Raman techniques and detected a bis-His species that occurs within the 100-μs dead time of their mixing apparatus.

The assignment of a 2-μs Fe(II)−Met80 ligation and a 50-μs Fe(II)−His26/33 coordination is supported by recent time-resolved magnetic circular dichroism (TRMCD) studies (unpublished results), which are much more sensitive to the axial ligation of the iron than TROA or TRCD methods (*46*). The results of these studies will be reported in a future publication. These assignments are also supported by TROA studies of the heme peptide of cyt*c* (*28*, *29*), where the time constants for free methionine and histidine binding to the heme were reported to be 3−4 and 120 μs, respectively.

Secondary Structure Changes. The results of the far-UV TRCD studies, with support from time-resolved fluorescence (TRFL) studies (*47*), indicate that the 50-μs process is not a transient molten globule intermediate whose secondary structure is similar to that in the native form (*48*). The far-UV TRCD data show only 7% of the near-native CD signal at 220 nm within 500 ns and 8% at 2 μs (Figure 6), after which there is no further increase in the magnitude of the signal. In TRFL studies of COCyt*c* no detectable changes in the Trp59 fluorescence signal were observed from 10 ns to 10 ms after photolysis (*47*). The detection of some signal in TRCD experiments and none in TRFL studies may reflect the sensitivity of CD measurements to global structural features and the sensitivity of fluorescence to local interactions.

According to Bushnell et al. (*49*), the high-resolution three-dimensional structure of horse heart oxCyt*c* shows the native protein secondary structure with three major [residues 6−14 (N-helix), 60−69 (60's helix), and 87−102 (C-helix)] and two minor (residues 49−54 and 70−75) helical sections that interact to form some tertiary structure. The results of H-exchange labeling and proton NMR studies, which characterized the structure of folding intermediates in oxCyt*c* (*50*), suggest that in the early stages of folding (<20 ms) the N- and C-terminal α-helical segments are present and are stabilized by helix−helix contacts. Thus, secondary structure formation at the N- and C-terminal helices may account for the observed 8% increase in TRCD signal of COCyt*c* at 2 μs, as was suggested for the ∼45% of secondary structure observed in the 4-ms dead time of stopped-flow CD experiments on oxCyt*c* (*10*). Because the heme group is involved in the contact between the N- and C-terminal regions of the folded protein (*49*, *51*), it is expected to play a role in the helix−helix association during the early stages of folding in oxCyt*c*. In fact, early interaction between the two terminal helices of oxCyt*c* is suggested to be accompanied by a polypeptide condensation (collapse) that leads to a ∼35% decrease of the initial Trp59 fluorescence

intensity within 4 ms (*10*) and an additional ~30% decrease within 20 ms (*50*). Therefore, contrary to the results of TRFL studies (*47*), some changes in the Trp59 fluorescence intensity on a sub-millisecond time scale would be expected.

On the basis of the above NMR, stopped-flow CD, and fluorescence studies, the absence of changes in the TRFL measurements and the 8% change in TRCD signal within 2 μs have several implications for COCyt*c* folding. First, the TRCD, as well as the TRFL (*47*), studies of COCyt*c* emphasize that the experimental conditions used in these studies destabilize the folding intermediates, as well as the native state, and favor the unfolded state of the protein. Evidence that the unfolded state is favored under these experimental conditions comes from photolysis of the COCyt*c* sample using a repetition rate of 5 Hz. COCyt*c* in 4.6 M GdnHCl (40 °C, pH 6.5) exhibited less than 20% of the native redCyt*c* CD signal at 220 nm upon photolysis, whereas the same experiments performed at room temperature show the appearance of 40% of the native redCyt*c*. Second, the 8% increase of the TRCD signal within 2 μs may be due to formation of structure at the N- and C-terminal helical segment. If we consider this result in terms of the total α-helix content, which is approximately 45% (*49*), then the two extreme interpretations of these results are that within 2-μs either 100% of the α-helix is present one-fifth of the time or that only ~15% of the total helix content is formed (see below). Third, if formation of, and contact between, these two major helices is accompanied by a decrease in the Trp59 fluorescence intensity (*8, 10*), then secondary structure formation may drive the reduction of the heme−Trp59 distance. This idea is consistent with the observation in these TRCD studies that by 500 ns 7% of the native secondary structure forms, before a Fe(II)−Met80 ligation process occurs at 2 μs. Finally, because the Trp fluorescence probes tertiary interactions with the heme group and nearby secondary structures, it is expected to be a very sensitive probe of polypeptide collapse. However, it is also a localized probe that is located at the periphery of one major helix (residues 60−69) and 5 residues away from a minor helical section (residues 49−54). Thus, with only 8% secondary structure there may not be sufficient helix formation or helix−helix contact to facilitate detectable changes in the Trp59 TRFL studies. These results also suggest that the 8% increase of the TRCD signal is due to formation of only 15% of the total helix content in cyt*c*, as opposed to the observation of 100% helix formation one-fifth of the time.

The assignment of the far-UV TRCD changes to secondary structure formation rather than heme or aromatic residue changes is based predominantly on the shape and the time scale of the signals. The spectral shapes of the TRCD signals are consistent with the initial-state CD spectrum that is characteristic of the secondary structure in native cyt*c*, even though the TRCD signals are limited to the 210−222-nm region. In addition, because most of the TRCD signal (7% at 500 ns) is detectable before the first two processes (2 and 50 μs) are observed, the contribution of heme ligation effects to these CD changes should be minimal. Detection of 7% global secondary structure within 500 ns is consistent with the results of recent nanosecond time-resolved infrared (TRIR) studies on apoMb folding (*24*). In these TRIR studies, which probe the time dependence of more localized secondary structure, a time constant ranging from 48 to 200 ns was assigned to the formation of solvated structure in either the C, D, or F helices in apoMb.

The offset of larger negative TRCD signals with positive TRCD features having similar kinetics to give the observed small CD changes was also considered. This situation can arise from contributions of aromatic residues in the far UV, which are particularly significant if the content of helix is low. Because the secondary structure of cyt*c* at 4.6 M GdnHCl is partly unfolded, aromatic residues may influence the far-UV TRCD signal with positive bands in the region between 215 and 235 nm (*52*). However, if this were the case, the TRCD spectra should reflect the convolution of positive bands around 215−230 nm.

It is also important to consider the influence of heme−protein interactions in the far-UV region because a corresponding increase in this coupling is expected as the protein folds. If we can draw parallels between folding around the heme and insertion of a heme group into a protein, then we can look to early studies of the Cotton effect in apoMb versus metmyoglobin (metMb) (*53*) to understand the heme−protein interaction in the far-UV region. Addition of heme to apoMb results in a larger CD signal at 222 nm, which is comparable to the signal for native metMb. The increase in CD signal for metMb was attributed to a change in helix content that is induced by the presence of the heme, rather than to coupling of the heme−peptide transitions. From CD as well as optical rotatory dispersion studies on Mb, it was suggested that heme transitions centered within 50−100 nm from the n−π* peptide transition may contribute to the optical rotation at 233 nm but will have much less influence on the CD measured at 222 nm. Thus, on the basis of this CD study of apoMb and the arguments of spectral shape and time scale of appearance, we suggest that the TRCD signals predominantly represent the initial stages of secondary structure formation.

The degree to which CO rebinding competes with the folding process was examined by repeating the COCyt*c* photolysis experiments in the far-UV region using 3:1, 8:1, and 16:1 ratios of Ar to CO gas. With a 16:1 Ar to CO ratio, the mixed-gas experiments were limited by the presence of CO-unbound redCyt*c*. When the earliest CO rebinding process was extended 8-fold, from 225 μs to 1.8 ms, there was no further increase in the magnitude of the TRCD signal at 220 nm. There are at least two possible reasons that additional changes in the far-UV TRCD data are not observed. First, folding of redCyt*c* is slow under the current experimental conditions (4.6 M GdnHCl, 40 °C, pH 6.5), which apparently destabilize both the native structure and the partially folded intermediates. An estimated folding rate constant of 1.3 s^{-1} has been reported for redCyt*c* in 4.6 M GdnHCl at pH 7 (*30*). This rate constant is similar to the folding rate of 1 s^{-1} obtained from stopped-flow experiments (unpublished results cited in ref *27*) where the GdnHCl concentration is jumped from 6 to 4.6 M. The effect of GdnHCl on the folding process is apparent when the folding rate in 4.6 M GdnHCl is compared to the estimated folding rate constant of 2×10^3 s^{-1} that is reported for redCyt*c* in 0.7 M GdnHCl (40 °C, pH 7) (*30*). Because the folding rate constant is so slow for redCyt*c* in 4.6 M GdnHCl, detection of only 8% folding is not unusual.

A second explanation for why additional folding is not observed beyond 2 μs or in the mixed-gas experiments is

that formation of the Fe(II)−His species at 50 μs may contribute to barriers against folding, until CO rebinds. A misligation through the Fe(II)−His is consistent with the results of recent rapid-mixing resonance Raman studies of oxCyt*c* folding (*40*, *45*). Although this comparison is between oxCyt*c* and COCyt*c*, they have comparable fractions of unfolded protein in their respective GdnHCl concentrations. In the resonance Raman study a bis-His species, which was proposed to compete with and to slow folding, was detected within the 100-μs dead time of their mixing apparatus. At low pH it is suggested that the folding rate of oxCyt*c* is accelerated because His26 and His33 are protonated, preventing the formation of bis-His intermediates (*8*, *38*−*42*). However, from MCD studies in this lab (unpublished results) it was shown that redCyt*c* in 4.6 M GdnHCl comprises 60% non-native Fe(II)−His and 40% Fe(II)−Met. Yet, according to far-UV CD studies, redCyt*c* maintains near-native secondary structure. How, then, does formation of Fe(II)−His inhibit folding? The data also raise the question of whether the near-native secondary structure or the bis-His ligation comes first in equilibrium redCyt*c*. Because mixed-gas experiments show no CD changes between the 50-μs Fe(II)−His formation and the 1.8-ms CO rebinding processes and no changes in the amplitudes of any of the four processes (Table 1), slow refolding due to the experimental conditions probably contributes more to the small TRCD changes.

COCyt*c Photolysis Mechanism.* The following three schemes, which are presented as possible mechanisms for the COCyt*c* photolysis reaction, are based on several results. First, as discussed above, the two species that bind CO differ in the interactions between the heme group and the protein. This is evidenced by the fact that the 225-μs process is not detected by near-UV TRCD and TROA methods, while the 880-μs process is consistently observed in all the TROA and TRCD studies (Table 1). Second, recent steady-state MCD measurements indicate that at 4.6 M GdnHCl (pH 6.5, 40 °C) the Fe(II) coordination in redCyt*c* is 60% bis-His and 40% His−Met. And finally, preliminary TRMCD studies (unpublished results) indicate that in the 2- and 50-μs processes Met and His, respectively, bind to a five-coordinate species. These results suggest a possible kinetic mechanism where photolysis of COCyt*c* generates two populations, one having a propensity to bind Met (U_{Met}*) and the other, to bind His (U_{His}*, mechanism I). The environment of U_{Met}* may facilitate the initial formation of secondary structure (U〰) that favors binding of the native Met80 ligand. Subsequently, CO displaces the Met and His ligands to reform U−CO.

Mechanism I

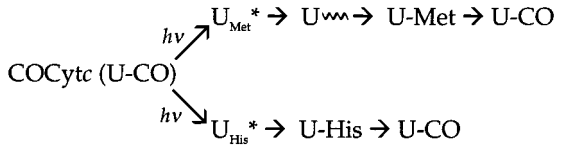

Whereas the results of steady-state MCD studies favor mechanism I, the near-UV TRCD and TROA data suggest a different scheme. Time-resolved near-UV results indicate that the first CO rebinding process (225 μs) does not have detectable heme−aromatic side-chain tertiary interactions, in contrast to the processes of Fe(II)−Met and Fe(II)−His formation (ca. 2 and 50 μs) and the second CO rebinding (ca. 800 μs). This difference in the heme tertiary interactions suggests formation of an unfolded photoproduct, U*, that only undergoes CO rebinding (mechanism II). If we assume the parallel formation of U* and U_{Met}* and a simple sequential step where His displaces Met from the heme, then CO will rebind U* and replace a His ligand.

Mechanism II

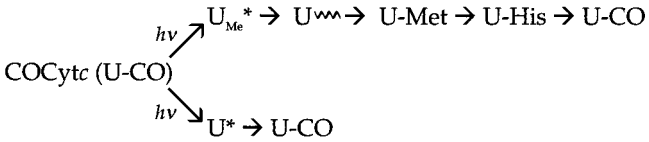

A variation of mechanism II might involve the parallel formation of U*, Fe(II)−Met, and Fe(II)−His (mechanism III). Displacement of the Met ligand by His is suggested by the k_{on}/k_{off} for Met65/80, which is approximately 0.1 (*28*), and the presence of both Fe(II)-Met and Fe(II)-His species in the initial-state sample of redCyt*c* (work in progress).

Mechanism III

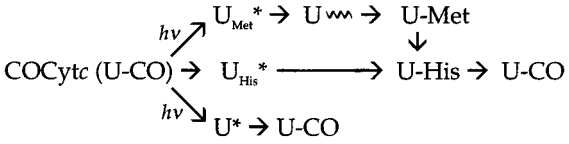

Currently, mechanism I is favored over mechanims II and III because preliminary TRMCD studies indicate that Met and His bind to five-coordinate species. Further work is in progress to try to establish in detail the mechanism of COCyt*c* photolysis.

ACKNOWLEDGMENT

We thank Drs. Robert Goldbeck, James Lewis, Youxian Wen, YiRen Gu Thomas, Daniel B. Kim-Shapiro, and Raymond Esquerra for helpful discussions, and Drs. Gary Martinez and Sangita Seshadri for advice concerning cytochrome *c* samples.

REFERENCES

1. Kauzmann, W. (1959) *Adv. Protein Chem. 14*, 1−64.
2. Mirsky, A. E., and Pauling, L. (1936) *Proc. Natl. Acad. Sci. U.S.A. 22*, 439−447.
3. Tsong, T. Y. (1974) *J. Biol. Chem. 249*, 1988−1990.
4. Kuwajima, K., Yamaya, H., Miwa, S., Sugai, S., and Nagamura, T. (1987) *FEBS Lett. 221*, 115−118.
5. Gilmanshin, R. I., and Ptitsyn, O. B. (1987) *FEBS Lett. 223*, 327−329.
6. Jeng, M.-F., Englander, S. W., Elöve, G. A., Wand, A. J., and Roder, H. (1990) *Biochemistry 29*, 10433−10437.
7. van Osdol, W. W., Mayorga, O. L., and Freire, E. (1991) *Biophys. J. 59*, 48−54.
8. Elöve, G. A., Bhuyan, A. K., and Roder, H. (1994) *Biochemistry 33*, 6925−6935.
9. Roder, H., and Elöve, G. A. (1994) in *Mechanisms of Protein Folding* (Pain, R. H., Ed.), pp 26−54, Oxford University Press, Oxford, U.K.
10. Elöve, G. A., Chaffotte, A. F., Roder, H., and Goldberg, M. E. (1992) *Biochemistry 31*, 6876−6883.

11. Varley, P., Gronenborn, A. M., Christensen, H., Wingfield, P. T., Pain, R. H., and Clore, G. M. (1993) *Science 260*, 1110−1113.
12. Lumry, R., Legare, R., and Miller, W. G. (1964) *Biopolymers 2*, 489.
13. Hamori, E., and Scheraga, H. A. (1967) *J. Phys. Chem. 71*, 4147−4150.
14. Hammes, G. G., and Roberts, P. B. (1969) *J. Am. Chem. Soc. 91*, 1812−1816.
15. Barksdale, A. D., and Stuehr, J. E. (1972) *J. Am. Chem. Soc. 94*, 3334−3338.
16. Cummings, A. L., and Eyring, E. M. (1975) *Biopolymers 14*, 2107−2114.
17. Bosterling, B., and Engel, J. (1979) *Biophys. Chem. 9*, 201−209.
18. Grunenewald, G., Nicola, C. U., Lustig, A., Schwarz, G., and Klump, H. (1979) *Biophys. Chem. 9*, 137−147.
19. Sano, T., and Yasunga, T. (1980) *Biophys. Chem. 11*, 377−386.
20. Williams, S., Causgrove, T. P., Gilmanshin, R., Fang, K. S., Callender, R. H., Woodruff, W. H., and Dyer, R. B. (1996) *Biochemistry 35*, 691−697.
21. Thompson, P. A. (1997) in *Techniques in Protein Chemistry* (Marshak, D. R., Ed.), Vol. VIII, Academic Press, San Diego, CA.
22. Ballew, R. M., Sabelko, J., and Gruebele, M. (1996) *Proc. Natl. Acad. Sci. U.S.A. 93*, 5759−5764.
23. Ballew, R. M., Sabelko, J., and Gruebele, M. (1996) *Nat. Struct. Biol. 3*, 923−926.
24. Gilmanshin, R., Williams, S., Callender, R. H., Woodruff, W. H., and Dyer, B. (1997) *Proc. Natl. Acad. Sci. U.S.A. 94*, 3709−3713.
25. Nölting, B., Golbik, R., and Fersht, A. R. (1995) *Proc. Natl. Acad. Sci. U.S.A. 92*, 10667−10672.
26. Phillips, C. M., Mizutani, Y., and Hochstrasser, R. M. (1995) *Proc. Natl. Acad. Sci. U.S.A. 92*, 7292−7296.
27. Jones, C. M., Henry, E. R., Hu, Y., Chan, C.-K., Luck, S. D., Bhuyan, A., Roder, H., Hofrichter, J., and Eaton, W. A. (1993) *Proc. Natl. Acad. Sci. U.S.A. 90*, 11860−11864.
28. Hagen, S. J., Hofrichter, J., and Eaton, W. A. (1997) *J. Phys. Chem. B 101*, 2352−2365.
29. Hagen, S. J., Hofrichter, J., Szabo, A., and Eaton, W. A. (1996) *Proc. Natl. Acad. Sci. U.S.A. 93*, 11615−11617.
30. Pascher, T., Chesick, J. P., Winkler, J. R., and Gray, H. B. (1996) *Science 271*, 1558−1560.
31. Mines, G. A., Pascher, T., Lee, S. C., Winkler, J. R., and Gray, H. B. (1996) *Chem. Biol. 3*, 491−497.
32. Zhang, C.-F., Farrens, D. L., Björling, S. C., Song, P.-S., and Kliger, D. S. (1992) *J. Am. Chem. Soc. 114*, 4569−4580.
33. Zhang, C.-F., Lewis, J. W., Cerpa, R., Kuntz, I. D., and Kliger, D. S. (1993) *J. Phys. Chem. 97*, 5499−5505.
34. Chen, E., and Kliger, D. S. (1996) *Inorg. Chim. Acta 242*, 149−158.
35. Chen, E., Lapko, V. N., Song, P.-S., and Kliger, D. S. (1997) *Biochemistry 36*, 4903−4908.
36. Henry, E. R., and Hofrichter, J. (1992) *Methods Enzymol. 210*, 129−192.
37. Goldbeck, R. A., and Kliger, D. S. (1993) *Methods Enzymol. 226*, 147−177.
38. Tsong, T. Y. (1975) *Biochemistry 14*, 1542−1547.
39. Stellwagen, E., and Babul, J. (1975) *Biochemistry 14*, 5135−5140.
40. Yeh, S.-R., Takahashi, S., Fan, B., and Rousseau, D. L. (1997) *Nat. Struct. Biol. 4*, 51−56.
41. Sosnick, T. R., Mayne, L., and Englander, S. W. (1996) *Proteins: Struct., Funct., Genet. 24*, 413−426.
42. Sosnick, T. R., Mayne, L., Hiller, R., and Englander, S. W. (1994) *Nat. Struct. Biol. 1*, 149−156.
43. Babul, J., and Stellwagen, E. (1971) *Biopolymers 10*, 2359−2361.
44. Colón, W., Wakem, L. P., Sherman, F., and Roder, H. (1997) *Biochemistry 36*, 12535−12541.
45. Takahashi, S., Yeh, S.-R., Das, T. K., Chan, C.-K., Gottfried, D. S., and Rousseau, D. L. (1997) *Nat. Struct. Biol. 4*, 44−50.
46. Dawson, J. H., and Dooly, D. M. (1989) in *Iron Porphyrins* (Lever, A. B. P., and Gray, H. B., Eds.) Part 3, chs 1−2, pp 1−131, VCH Publishers, New York, NY.
47. Chan, C.-K., Hofrichter, J., and Eaton, W. A. (1996) *Science 274*, 628−629.
48. Ohgushi, M., and Wada, A. (1983) *FEBS Lett. 164*, 21−24.
49. Bushnell, G. W., Louie, G. V., and Brayer, G. D. (1990) *J. Mol. Biol. 214*, 585−595.
50. Roder, H., Elöve, G. A., and Englander, S. W. (1988) *Nature 335*, 700−704.
51. Takano, T., and Dickerson, R. E. (1981) *J. Mol. Biol. 153*, 79−94.
52. Woody, R. W. (1994) in *Circular Dichroism: Principles and Applications* (Nakanishi, K., Berova, N., and Woody, R. W., Eds.) pp 473−496, VCH Publishers, New York, NY.
53. Breslow, E., Beychok, S., Hardman, K. D., and Gurd, G. R. N. (1965) *J. Biol. Chem. 240*, 304−309.

BI972369F